Hindawi
Journal of Advanced Transportation
Volume 2024, Article ID 9967121, 14 pages
https://doi.org/10.1155/2024/9967121

Research Article

Modified Model Predictive Control for Coordinated Signals along an Arterial under Relaxing Assumptions

Kun Zhang, Hongfeng Xu, Baofeng Pan, Qiming Zheng, and Hongjin Chen

Department of Transportation and Logistics, Dalian University of Technology, Dalian 116024, China

Correspondence should be addressed to Kun Zhang; zhangkun93@mail.dlut.edu.cn and Hongfeng Xu; hfxu@dlut.edu.cn

Received 26 September 2023; Revised 2 February 2024; Accepted 7 February 2024; Published 21 February 2024

Academic Editor: Jinjun Tang

This paper proposes modified model predictive control (MMPC) for coordinated signals, aiming to enhance a model's fidelity to the realistic traffic environment by relaxing typical assumptions. We focus on the arterial, where every intersection is equipped with a dual-ring-barrier signal controller that complies with the standards of the National Electric Manufacturers Association. MMPC employs the store-and-forward model to describe traffic flow, thereby transforming the signal control problem into a model-based rolling-horizon optimization problem, in which the prediction horizon is composed of several future sample intervals, commonly equal to the cycle length. A radar detector is used to collect vehicle data upstream of the stop line at every sampling instant. The optimization problem is solved to minimize the number of vehicles within the prediction horizon, and the next timing plan is determined based on the optimization results. Constraints are added and modified in order to incorporate the typical relaxed assumptions in the optimization process. For this purpose, MMPC introduces a transition-free ring-barrier structure, vehicle distribution ratio, and percent arrival before the end of green. Simulation results indicate that coordination can be maintained by MMPC without the need for transitions, and the estimation of current and future traffic states can be improved with the assistance of modified constraints. Compared with benchmark techniques, MMPC offers superior vehicle progression for coordinated movement and significant improvements in delays, number of stops, and total travel time from a system-wide perspective, with an acceptable small increase in runtime.

1. Introduction

The arterial serves as a major roadway that connects adjacent urban functional areas. Signals are operated as a group to provide a good progression in the high-priority direction, known as the coordinated direction. Although the arterial is part of the traffic network, arterial coordinated signal control and regional signal control are two distinct techniques, with the most significant difference being that coordinated signal control along the arterial not only considers overall performance but also emphasizes coordination progression.

Arterial coordinated signal control techniques can be classified into fixed-time, actuated, and adaptive control. In fixed-time control, a fixed green time is unable to accommodate demand fluctuations and to create a timing plan involves substantial investment and engineering judgment. Actuated control is an extension of fixed-time control that incorporates actuated logic, thus relying heavily on the quality of the timing plan. Furthermore, the issue of early return to green inevitably disrupts vehicle movement in the coordinated direction [1, 2]. In contrast to the aforementioned techniques, adaptive control typically involves the definition of control objectives and objective functions, treating the adjustment of signal timing to real-time traffic states as an optimization problem. Adaptive control, as an advanced technology for arterial coordinated signal control, significantly reduces the need for engineering judgment in the control process.

Model predictive control (MPC) is an advanced process control method that has demonstrated its superiority through numerous industrial applications [3]. Many attempts have been made to apply MPC to signal control, which falls within the scope of adaptive control by definition [4]. The three fundamental elements of MPC are the predictive model, objective function, and rolling optimization [5]. The signal control problem can be transformed into a model-based rolling-horizon optimization problem [6, 7], where the prediction horizon is composed of several future sample intervals, commonly the cycle length. The prediction model, based on a macroscopic traffic flow model, deduces future traffic states from the current states and the future timing plan. The objective function is constructed based on the traffic states within the prediction horizon. At every sampling instant, the optimization problem is solved online to generate a sequence of timing plans corresponding to the predicted horizon, and the first timing plan in the sequence is executed, in a process referred to as rolling optimization. The MPC provides a robust framework for signal control, allowing cycle-by-cycle adjustments to varying traffic states.

Traditional MPC primarily targets the network level, relying on strong assumptions about the research environment, including one-way streets, disregarded pedestrian demand, and the absence of complex phase structures, which can enable easier and faster solutions. However, the resulting prediction models can significantly deviate from the realistic traffic environment, leading to inaccurate predictions of future traffic states, irrational timing plans, and potential implementation obstacles. For this purpose, this paper relaxes the assumptions and proposes a modified model predictive control (MMPC) for coordinated signals along an arterial. The main contributions are as follows:

(1) By analyzing the typical assumptions in traditional MPC, this study proposes relaxed assumptions approximating the realistic traffic environment, addressing problem in the traditional MPC.

(2) The introduction of the transition-free ring-barrier structure makes the MMPC can maintain the offset of the coordinated phases without transition, which provides a great vehicle progression for the coordinated movement.

(3) A mechanism for estimating the number of vehicles for a phase is introduced, and this estimation is minimally influenced by the timing plan. This modification allows the MMPC to more accurately perceive the traffic state.

(4) The introduction of the percent arrival before the end of green in MMPC prevents the wastage of green time caused by the inability of the inflow to arrive, and eliminates the disturbance of this phenomenon on the estimation of the number of vehicles.

(5) The results of simulation experiments show that the MMPC method significantly improves the delay, number of stops, and total travel time while maintaining coordination compared to the traditional MPC method as well as other benchmark methods.

2. Literature Review

Numerous studies have been conducted on the application of MPC to traffic signal control, with a particular focus on the network level. Researchers have attempted to increase the operational efficiency of MPC by investigating control architectures, macroscopic traffic flow models, and assumptions, to make it applicable to larger and more complex traffic networks.

MPC can be categorized into distributed and centralized architectures, depending on the control architecture. The advantage of centralized architecture is that the control center can optimize the problem globally to find the global optimal solution, and determine the timing plans for all of the intersections. However, faced with large-scale traffic networks, the computational complexity of centralized architectures increases dramatically, resulting in unacceptable runtimes. Conversely, distributed architectures can significantly decrease the overall runtime by decomposing the problem into multiple subproblems and allocating the computations to the signal controllers, thereby reducing the communication load and computational complexity of the key nodes [8, 9]. However, its performance is inferior to that of the centralized architecture [10–13]. Each architecture has its own specific focus and suitable applications. The adoption of a centralized architecture in arterial traffic systems is common, feasible, and necessary [13, 14].

The macroscopic traffic flow model encompasses the researchers' understanding of the realistic traffic environment. It plays a crucial role in the prediction model, directly impacting the performance and computational complexity of MPC. Among such models, MPC commonly employs the store-and-forward model (SFM) and cellular transport model (CTM) [14]. A key characteristic of SFM is its ability to model traffic flows using a simplified mathematical description, eliminating the need for discrete variables during optimization. This model has paved the way for optimization problems with polynomial complexity and has found practical applications in realistic networks [15, 16]. In contrast to SFM, CTM divides links into smaller segments, enabling a more precise representation of non-uniform traffic states within every segment. Smaller segments necessitate shorter sampling intervals, which have minimal impact in traffic networks, but increase model complexity [17]. Therefore, SFM is considered more suitable than CTM for traffic networks.

Assumptions are employed to simplify and abstract the complex nature of the realistic traffic environment, aiming to facilitate the solution of MPC. The assumptions that follow are common in MPC in the field of signal control, either explicit or implicit, as shown in Table 1. However, these assumptions are excessively strong, and they significantly increase the deviation of the model from realistic traffic. Although some assumptions can be relaxed through simple extensions based on existing research, it should be noted that to achieve complex phase structures and offset transitions in existing studies, it inevitably requires structural modifications. The purpose of these assumptions is to eliminate nonessential confounding factors from the research, enabling a more focused investigation of the core problem. However, in the case of network-level MPC, current research places a greater emphasis on the methodology, often customizing assumptions to conform to it. Therefore, the objective of this paper is to reassess the role of assumptions in signal control and restore a realistic traffic environment for arterials.

Table 1: Typical assumptions.

ID	Typical assumptions	Literature number
1	All of the streets are one-way, intersections are abstracted as nodes, and traffic channelization is not taken into account	[18–22]
2	Vehicle demand is the sole consideration in traffic demand, and pedestrian crossing demand is not taken into account	[6, 15–30]
3	Traffic signal controllers can only accommodate two or four phases and do not support complex phase structures (e.g., phase overlap)	[28–32]
4	The offset of every intersection is set to 0, and the offset transition is not taken into account	[20, 21, 23, 28, 31]
5	The turning ratio at every approach remains constant and known, with turning vehicles uniformly distributed over the link	[6, 17, 20, 27]
6	Vehicles entering the link can pass the stop line during the current cycle	[6, 16, 17, 26, 27]

To summarize, traditional network-level MPC methods are deemed unsuitable for arterials. Due to the key characteristics of arterials, i.e., a limited number of intersections and simple relationships, they have low requirements for control architectures and macroscopic traffic flow models. Hence, the increase in computational complexity resulting from the relaxation of typical assumptions is acceptable. We aim to restore the realistic traffic environment of arterials by relaxing typical assumptions, thereby facilitating the implementation of MPC.

3. Assumptions

The assumptions proposed in this paper, along with the differences from typical assumptions, are presented in Table 2. Assumptions 1–3 each play a role in approximating the traffic environment, corresponding to traffic channelization, traffic demand, and signal controller types, respectively. Assumptions 4–6 represent the fundamental understanding of the realistic traffic environment by MMPC control techniques, corresponding respectively to offset configuration, turning ratio, and vehicle passage conditions.

For convenience, in this paper, the coordination direction is set from west to east.

4. Base Traffic Predictive Model

The traffic flow prediction model, which encompasses various constraints and traffic flow models, serves as a key component of MPC. Under typical assumptions, signal controllers operate in a stage-based manner, accommodating only two or four phases. The link is chosen as the control object, and the number of vehicles (referred to as queues in some studies) within the link is considered the state variable. The prediction of the number of vehicles within the link is then conducted using the time constraints of every stage, the storage capacity constraints of the link, and the traffic flow model. Because the stage-based structure is not compatible with the NEMA standard, Wang and Abbas proposed an MPC method for NEMA-compliant signal controllers [27]. A traffic flow prediction model is established in this method, with phase as the control object, by introducing the concept of virtual phase links. By modifying this model, we create the basic traffic flow prediction model of this paper, which incorporates constraints related to green time, the number of vehicles, and the store-and-forward model. Table 3 summarizes the important variables used in this paper.

4.1. Green Time Constraints. The NEMA standard defines the organization of phases using rings and barriers [33], which also impose green time constraints. In the ring-barrier phase structure, a ring represents a sequence of conflicting phases, while a barrier indicates the point at which the phases in each ring must end simultaneously. For example, in a conventional four-leg intersection, there are four through phases and four protected left-turn phases, which are numbered as depicted in Figure 1. Moreover, according to NEMA standards, right-turn movements are typically permitted and are combined with through movements [33]. The ring-and-barrier diagram, as illustrated in Figure 2, imposes the following constraints on $S_{i,\mathrm{K}j}(n)$:

$$S_{i,\mathrm{K1}}(n) + S_{i,\mathrm{K2}}(n) = S_{i,\mathrm{K5}}(n) + S_{i,\mathrm{K6}}(n) = C_{i,\mathrm{ma}}(n), \tag{1}$$

$$S_{i,\mathrm{K3}}(n) + S_{i,\mathrm{K4}}(n) = S_{i,\mathrm{K7}}(n) + S_{i,\mathrm{K8}}(n) = C_{i,\mathrm{mi}}(n), \tag{2}$$

$$C_{i,\mathrm{ma}}(n) + C_{i,\mathrm{mi}}(n) = C(n), \tag{3}$$

where

$$S_{i,\mathrm{K}j}(n) = G_{i,\mathrm{K}j}(n) + R + Y. \tag{4}$$

The start time of a timing plan is introduced and defined as the start of the first phase in the phase sequence. As the cycle length represents the duration of a complete phase sequence, a recursive relationship arises:

$$\mathrm{STP}_i(n+1) = \mathrm{STP}_i(n) + C(n). \tag{5}$$

The offset reference point is utilized to establish the relationship between the coordinated phases along the arterial. The offset reference selected in this paper is the beginning of the first coordinated phase green, as defined officially in NTCIP 1202 [33]. $\mathrm{OR}_i(n)$ is given by

$$\mathrm{OR}_i(n) = \begin{cases} \mathrm{STP}_i(n), & \text{K2 is leading,} \\ \mathrm{STP}_i(n) + S_{i,\mathrm{K1}}(n), & \text{K2 is lagging.} \end{cases} \tag{6}$$

The minimum green and maximum green constraints are applied to $G_{i,\mathrm{K}j}(n)$ as follows:

Table 2: Assumptions and differences from typical assumptions.

ID	Assumptions	Differences
1	All streets are two-way, and traffic channelization is taken into account	Streets changed from one-way to two-way, and consideration of traffic channelization introduced
2	Traffic demand simultaneously takes into account both the vehicle demand and pedestrian crossing demand	Inclusion of pedestrian crossing demand in addition to vehicle demand
3	A dual-ring-barrier, eight-phase signal controller, as specified in the National Electric Manufacturers Association (NEMA) standards, is installed at every intersection	Transition from simpler signal controllers to more common types (NEMA standards) that support more phases and functions
4	The offset of every intersection is determined using alternative methods, taking into account the offset transition	Change in the determination of offset, now considering alternative methods and offset transition
5	The turning ratio randomly fluctuates within a certain range, and turning vehicles are not uniformly distributed over the link	Introduction of variability in turning ratios and non-uniform distribution of turning vehicles
6	Some of the vehicles entering the link cannot pass the stop line during the current cycle	Recognition that not all vehicles can pass the stop line during the current cycle, aligning with the practical reality that some vehicles must wait until the next cycle

Table 3: Variables and their descriptions.

Variable	Description
$\alpha_{i,\mathrm{K}j}(n)$	Percent arrival before the end of green of the n^{th} cycle for phase Kj at the i^{th} intersection
$C(n)$	Cycle length of the n^{th} cycle along the arterial
$C_{i,\mathrm{ma}}(n)$, $C_{i,\mathrm{mi}}(n)$	Cycle length of the n^{th} cycle for the major and minor street phases at the i^{th} intersection
$\mathrm{EG}_{i,\mathrm{K}j}(n)$	Efficient green time of the n^{th} cycle for phase Kj at the i^{th} intersection
$G_{i,\mathrm{K}j}(n)$	Green time of the n^{th} cycle for phase Kj at the i^{th} intersection
$\mathrm{Min}\,G_{i,\mathrm{K}j}$, $\mathrm{Max}\,G_{i,\mathrm{K}j}$	Minimum and maximum green, respectively, for phase Kj at the i^{th} intersection
N_{h}, N_{p}	Historical and predictive horizon, respectively
$\mathrm{OR}_i(n)$	Offset reference point of the n^{th} cycle for the i^{th} intersection
$\mathrm{QS}_{i,\mathrm{K}j}$	Queue service time for phase Kj at the i^{th} intersection
$r_{i,\mathrm{K}j}$	Vehicle distribution ratio for phase Kj at the i^{th} intersection
R, Y	Red clearance interval and yellow change interval, respectively
$S_{i,\mathrm{K}j}(n)$	Split time of the n^{th} cycle for phase Kj at the i^{th} intersection
$\mathrm{SC}_{i,\mathrm{K}j}$	Storage capacity for phase Kj at the i^{th} intersection
$\mathrm{SFR}_{i,\mathrm{K}j}$	Saturation flow rate for phase Kj at the i^{th} intersection
$\mathrm{STP}_i(n)$	Start time of the timing plan of the n^{th} cycle for the i^{th} intersection
$V^{\mathrm{in}}_{i,\mathrm{K}j}(n)$, $V^{\mathrm{out}}_{i,\mathrm{K}j}(n)$	Inflow and outflow of the n^{th} cycle for phase Kj at the i^{th} intersection
$X_{i,\mathrm{K}j}(n)$	Number of vehicles of the n^{th} cycle for phase Kj at the i^{th} intersection

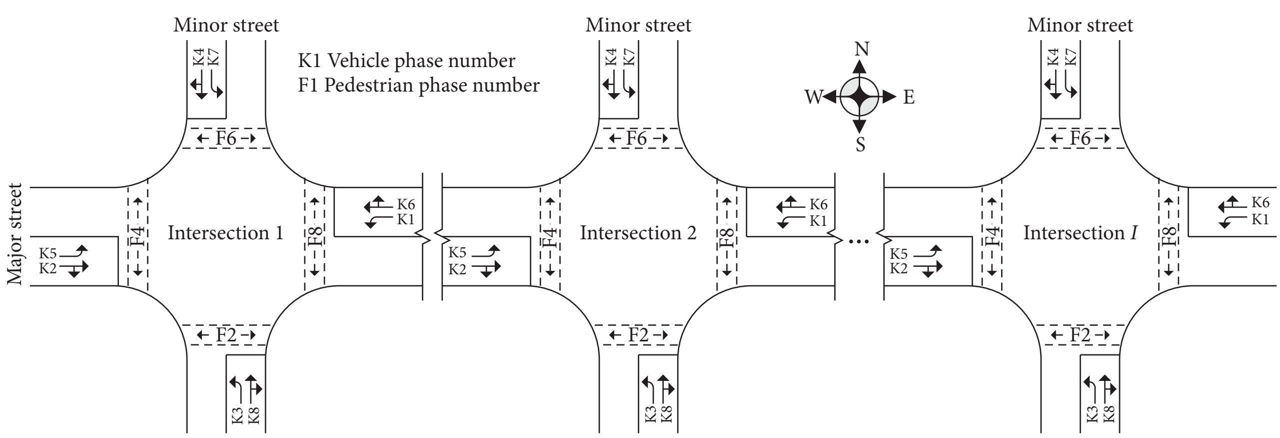

Figure 1: MMPC-enabled arterial and intersections illustrated.

$$\mathrm{Min}\,G_{i,\mathrm{K}j} \le G_{i,\mathrm{K}j}(n) \le \mathrm{Max}\,G_{i,\mathrm{K}j}. \tag{7}$$

4.2. Constraints on Number of Vehicles. The number of vehicles for a phase serves as the state variable of MPC, reflecting the traffic state of that phase, and is subject to a constraint:

$$0 \le X_{i,\mathrm{K}j}(n) \le \mathrm{SC}_{i,\mathrm{K}j}. \tag{8}$$

Because vehicles occupy similar lengths in every lane, the storage capacity of the phases depends on their corresponding zones, which include the approach lanes and upstream links. In contrast to the approach lanes, an upstream link serves as a shared zone for all of the phases in the approach. The storage capacity is commonly allocated as

$$\mathrm{SC}_{i,\mathrm{K}j} = N^{\mathrm{app}}_{i,\mathrm{K}j} \times \frac{L^{\mathrm{app}}_{i,\mathrm{K}j}}{L_{\mathrm{car}}} + r_{i,\mathrm{K}j} \times N^{\mathrm{link}}_{i,\mathrm{K}j} \times \frac{L^{\mathrm{link}}_{i,\mathrm{K}j}}{L_{\mathrm{car}}}, \tag{9}$$

where $r_{i,\mathrm{K}j}$ is replaced by the given turning rate for phase Kj at the i^{th} intersection; $L_{i,\mathrm{K}j}$ and $N_{i,\mathrm{K}j}$, respectively, represent the length and number of lanes of the designated zones for phase Kj at the i^{th} intersection; superscripts $(\cdot)^{\mathrm{app}}$ and $(\cdot)^{\mathrm{link}}$ indicate that a designated zone corresponds to an approach lane or upstream link, respectively; and L_{car} is the average length of a vehicle.

Similar to (9), $X_{i,\mathrm{K}j}(n)$, the initial number of vehicles for a phase, is calculated based on $r_{i,\mathrm{K}j}$ and the number of vehicles detected in the approach lanes and upstream links.

4.3. Store-and-Forward Model. The key idea of the store-and-forward model is vehicle conservation; this means that the future state is determined by both the current state and the change of state. Thus, the dynamics of phase Kj is given by the conservation equation:

$$X_{i,\mathrm{K}j}(n+1) = X_{i,\mathrm{K}j}(n) + V^{\mathrm{in}}_{i,\mathrm{K}j}(n) - V^{\mathrm{out}}_{i,\mathrm{K}j}(n). \tag{10}$$

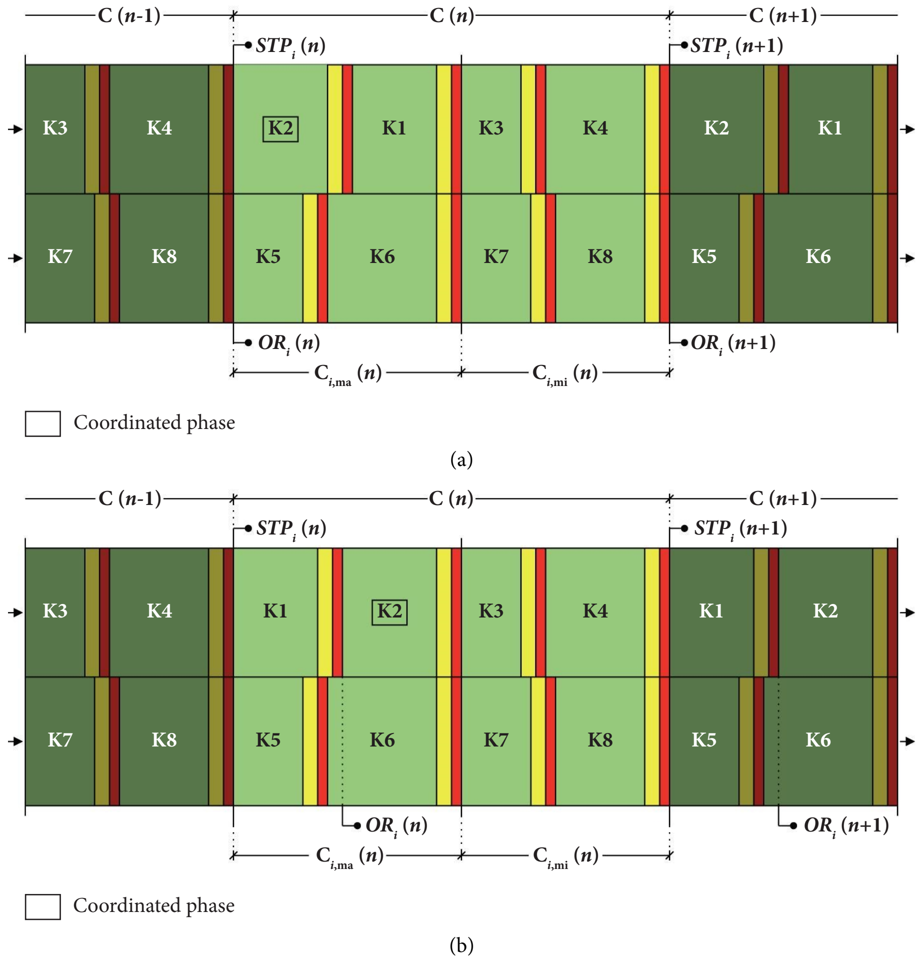

Figure 2: Ring-and-barrier diagram. (a) K2 is leading. (b) K2 is lagging.

The green time and saturation flow rate are commonly used to simplify the calculation of the outflow for the phase in order to avoid exponential growth in computational complexity. However, maintaining the saturation flow rate for the entire green time period is challenging. Therefore, the independent variable $\mathrm{EG}_{i,\mathrm{K}j}(n)$ is introduced to represent the efficient green time [17, 27], such that

$$V_{i,\mathrm{K}j}^{\mathrm{out}}(n) = \mathrm{EG}_{i,\mathrm{K}j}(n) \times \mathrm{SFR}_{i,\mathrm{K}j}, \tag{11}$$

$$0 \le \mathrm{EG}_{i,\mathrm{K}j}(n) \le G_{i,\mathrm{K}j}(n). \tag{12}$$

The inflow is classified into different cases depending on the presence or absence of upstream signals within the study area. $V_{i,\mathrm{K}j}^{\mathrm{in}}(n)$ is given by

$$V_{i,\mathrm{K}j}^{\mathrm{in}}(n) = \begin{cases} r_{i,\mathrm{K}j} \times \displaystyle\sum_{(x,\mathrm{K}y)\in \mathrm{PS}_{i,\mathrm{K}j}^{\mathrm{in}}}^{n} \left(t_{x,\mathrm{K}y,i} \times V_{x,\mathrm{K}y}^{\mathrm{out}}(n)\right), & \mathrm{PS}_{i,\mathrm{K}j}^{\mathrm{in}} \neq \varnothing, \\ C(n) \times \mathrm{AR}_{i,\mathrm{K}j}, & \mathrm{PS}_{i,\mathrm{K}j}^{\mathrm{in}} = \varnothing, \end{cases} \tag{13}$$

where $\mathrm{PS}_{i,\mathrm{K}j}^{\mathrm{in}}$ is the set of intersections and phases from which the outflows directly enter phase Kj at the i^{th} intersection; $t_{x,\mathrm{K}y,i}$ is the turning rate from phase Ky from the x^{th} to i^{th} intersection; and $\mathrm{AR}_{i,\mathrm{K}j}$ is the rate of vehicles entering phase Kj at the i^{th} intersection.

5. Transition-Free Ring-Barrier Structure

The transition is a necessary process of changing from one timing plan to another in the arterial [33–35]. It plays a key role in maintaining progression opportunities to the coordinated movement. The transition is commonly completed within one to five cycles, and frequent adjustments of the timing plan may result in a situation where the negative impacts of the transition outweigh the benefits of the new timing plan [33, 34].

The cycle length is consistent among all of the intersections in the arterial. Therefore, according to the conventional definition of cycle length, the start time of the timing plan at every intersection remains constant, and the offset reference points are determined through equations (5) and (6). Transition is required to adjust the start time of the timing plan and thereby maintain the relative relationship between the offset reference points along the arterial.

However, in the transition-free structure, the cycle length is redefined as the duration between two offset reference points, thereby preserving the relative relationship. The offset reference points exhibit a recursive relationship:

$$\mathrm{OR}_i(n+1) = \mathrm{OR}_i(n) + C(n). \tag{14}$$

For simplicity, the phases within the n^{th} cycle are denoted as light parts, as illustrated in Figure 3. This includes the phase between the offset reference points on the ring with the coordinated phase and between the start time of the timing plan on the other ring. When the coordinated phase is leading, the start time of the timing plan aligns with the offset reference point. Therefore, the distinction from existing research lies in the case where the coordinated phase lags behind.

$\mathrm{STP}_i(n)$ is given by

$$\mathrm{STP}_i(n) = \begin{cases} \mathrm{OR}_i(n), & \text{K2 is leading}, \\ \mathrm{OR}_i(n) - S_{i,\mathrm{K1}}(n-1), & \text{K2 is lagging}. \end{cases} \tag{15}$$

The original cycle length constraints for major streets and intersections, i.e., (1) and (3), require respective modifications as follows:

$$\begin{aligned} C_{i,\mathrm{ma}}(n) &= S_{i,\mathrm{K5}}(n) + S_{i,\mathrm{K6}}(n) \\ &= \begin{cases} S_{i,\mathrm{K1}}(n) + S_{i,\mathrm{K2}}(n), & \text{K2 is leading}, \\ S_{i,\mathrm{K1}}(n-1) + S_{i,\mathrm{K2}}(n), & \text{K2 is lagging}, \end{cases} \end{aligned} \tag{16}$$

$$C(n) = \begin{cases} C_{i,\mathrm{ma}}(n) + C_{i,\mathrm{mi}}(n), & \text{K2 is leading}, \\ S_{i,\mathrm{K2}}(n) + C_{i,\mathrm{mi}}(n) + S_{i,\mathrm{K1}}(n), & \text{K2 is lagging}. \end{cases} \tag{17}$$

6. Vehicle Distribution Ratio

Being a shared zone for all of the phases in the approach, the storage capacity, vehicles, and inflow should be distributed to these phases from the upstream link. Currently, there are two common ways to obtain the vehicle distribution ratio. One is to directly utilize the given turning rate, such as in typical assumption 5, but this ignores the stochastic nature of traffic demand. The other uses the number of departing vehicles, but this ignores the influence of timing plans.

For the real-time detection of phase demand, the phase vehicle weight $W_{i,\mathrm{K}j}(n)$ is constructed based on the number of departing and queued vehicles. This considers both the undersupply and oversupply of green time, thereby making traffic demand estimation nearly independent of timing plans. The phase vehicle weight is

$$W_{i,\mathrm{K}j}(n) = \max \begin{cases} \mathrm{ND}_{i,\mathrm{K}j}\left(\mathrm{STP}_i(n), \mathrm{STP}_i(n+1)\right), \\ \mathrm{NQ}_{i,\mathrm{K}j}(n), \end{cases} \tag{18}$$

where $\mathrm{ND}_{i,\mathrm{K}j}(t1, t2)$ is the number of departing vehicles during time period $[t1, t2]$ for phase $\mathrm{K}j$ at the i^{th} intersection and $\mathrm{NQ}_{i,\mathrm{K}j}(n)$ is the maximum number of queuing vehicles during the n^{th} cycle for phase $\mathrm{K}j$ at the i^{th} intersection, which can be obtained from detectors. Note that when calculating $W_{i,\mathrm{K}j}(n)$, if $\mathrm{STP}_i(n+1)$ has not been reached, the current system clock can be used as a substitute.

The expressions for $r_{i,\mathrm{K}j}(n)$ and its estimator $\hat{r}_{i,\mathrm{K}j}$ are

$$r_{i,\mathrm{K}j}(n) = \frac{W_{i,\mathrm{K}j}(n)}{\sum_{\mathrm{K}y \in \mathrm{PS}_{i,\mathrm{K}j}^{\mathrm{app}}} W_{i,\mathrm{K}y}(n)}, \tag{19}$$

$$\hat{r}_{i,\mathrm{K}j} = \frac{1}{N_h} \sum_{n=n_c-N_h+1}^{n_c} r_{i,\mathrm{K}j}(n), \tag{20}$$

where $\mathrm{PS}_{i,\mathrm{K}j}^{\mathrm{app}}$ is the set of phases in the same approach at phase $\mathrm{K}j$ and n_c is the current cycle number.

7. Percent Arrival before End of Green

In the store-and-forward model, the green time directly impacts the outflow, which is determined by the current number of vehicles and the inflow, with a theoretical upper limit.

Current research usually assumes that all of the inflow will be able to pass the stop line within the cycle, i.e., typical assumption 6. When the phase will display green or when the inflow will arrive within the cycle is not taken into account. This assumption contradicts reality and is replaced by assumption 6.

The percent arrival before the end of green ($\alpha_{i,\mathrm{K}j}(n)$) represents the partial inflow that can pass the stop line before the end of green in the n^{th} cycle for phase $\mathrm{K}j$, expressed as a percentage of the total inflow. It assumes that the inflow can travel at the speed limit without being

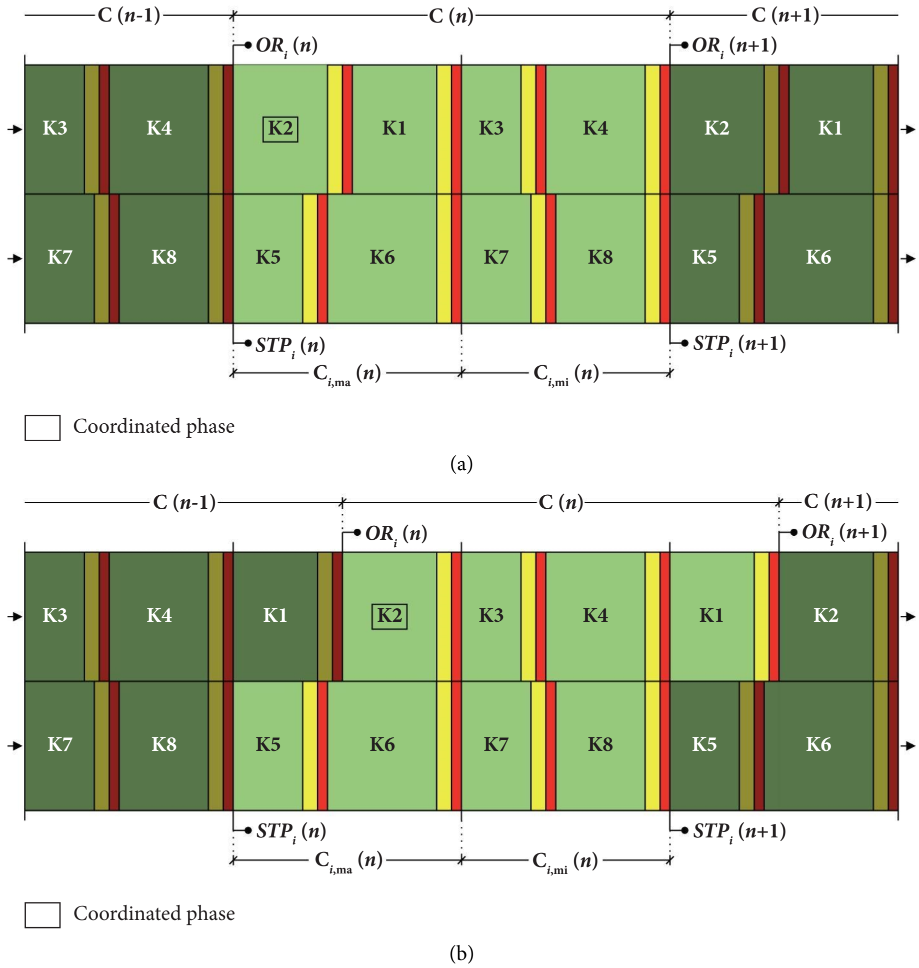

Figure 3: Ring-and-barrier diagram for MMPC. (a) K2 is leading. (b) K2 is lagging.

affected by other vehicles. This variable can precisely constrain the number of vehicles, but it requires much data, such as timing plans of the current and adjacent intersections, which significantly increases the complexity of the solution. To simplify the calculation, the future percentage is predicted by utilizing the percent arrival of the past N_{h} cycles:

$$\alpha_{i,\mathrm{K}j}(n) = \frac{\mathrm{NV}_{i,\mathrm{K}j}\left(n, \min\left(\mathrm{AEG}_{i,\mathrm{K}j}(n) - tt, \mathrm{STP}_i(n+1)\right)\right)}{\mathrm{NV}_{i,\mathrm{K}j}\left(n, \mathrm{STP}_i(n+1)\right)}, \tag{21}$$

$$\hat{\alpha}_{i,\mathrm{K}j} = \frac{1}{N_{\mathrm{h}}} \sum_{n=n_c-N_{\mathrm{h}}+1}^{n_c} \alpha_{i,\mathrm{K}j}(n), \tag{22}$$

where $\mathrm{NV}_{i,\mathrm{K}j}(n,t)$ is the cumulative number of vehicles passing in the upstream section for phase Kj at the i^{th} intersection from $\mathrm{STP}_i(n)$ to time t; $\mathrm{AEG}_{i,\mathrm{K}j}(n)$ is the actual end of green for phase Kj at the i^{th} intersection; tt is the travel time of vehicles from the upstream section to the stop line at the speed limit; and n_c is the current cycle number.

Hence, the original constraint (8) on the number of vehicles must be modified to

$$\left(1 - \hat{\alpha}_{i,\mathrm{K}j}\right) V^{\mathrm{in}}_{i,\mathrm{K}j}(n) \le X_{i,\mathrm{K}j}(n+1) \le \mathrm{SC}_{i,\mathrm{K}j}. \tag{23}$$

8. Simulation Experiments

An idealized arterial, consisting of three four-leg intersections, was simulated using Vissim 6.00-19. Two experiments were conducted to compare the MMPC with benchmark control techniques in terms of control objectives and operational performance. The benchmark control techniques include fixed-time control (FTC), semi-actuated control (SAC), and base model predictive control (BMPC). The control techniques in this paper were implemented using Python and the Vissim COM interface. For a more detailed description of the simulation experiment configuration, see reference [36].

8.1. Road Geometry. In Figure 1, intersections 1–3 are closely spaced, from west to east. Except for these intersections, there are no entrances and exits along the arterial. The posted speed limit remains at 50 km/h, while the desired free-flow speed follows a uniform distribution ranging from 48 to 58 km/h.

The intersections, as shown in Figure 4, share identical geometric designs and traffic control devices. Radar sensors are installed on the roadside to collect raw data (position and speed) from the stop line up to 130 m upstream [37–39]. Variables such as the number of queued vehicles and the number of vehicles in the approach lanes can be derived from the raw data. In addition, virtual loop detectors can be created from the raw data, positioned 40 m upstream of the stop lines for SAC [40].

8.2. Traffic Demand. To replicate the demand patterns during the heavy load scenarios of the day, the total simulation period (11700 s) was divided into three demand loading periods: 0–2700, 2700–9900, and 9900–11700 s. For every simulation run, a random sample of the traffic demand was taken at the start of the demand loading period. The sampling ranges are shown in Tables 4 and 5. Vehicle inputs contained only passenger cars.

8.3. Signal Timing Values. The cycle length was calculated using the Webster model, and the green time of phases for FTC was calculated based on the critical flow ratio of phases, as presented in Table 6. The result was also used as the background green time for the SAC and as the initial green time for BMPC and MMPC.

The other shared parameters are as follows:

(1) FTC, SAC, BMPC, and MMPC: $C(n) = 101$ s; $Y = 3$ s; $R = 2$ s; and $\mathrm{Min}\, G_{i,\mathrm{K}j} = 10$ s (K2 and K6), 14 s (K4 and K8), and 8 s (K1, K3, K5, and K7).

(2) BMPC and MMPC: $\mathrm{Max}\, G_{i,\mathrm{K}j} = 40$ s (K2 and K6), 44 s (K4 and K8), and 38 s (K1, K3, K5, and K7); $\mathrm{SFR}_{i,\mathrm{K}j} = 1900$ pcu/h; $N_\mathrm{h} = 5$; $N_\mathrm{p} = 5$; and $L_\mathrm{car} = 5$ m.

The lag-lag left-turn sequence was employed on the minor streets for all of the control techniques. Unless specified otherwise, the major street at intersection 1 set phases K2 and K5 as leading phases, intersection 2 set phases K1 and K5, and intersection 3 set phases K1 and K6. Two benchmark control techniques were employed using BMPC, referred to as BMPC-A and BMPC-B. BMPC-A defines the leading phases as described above, while BMPC-B modifies the leading phases of all of the major streets to phases K2 and K5. BMPC-B was exclusively employed for experiment 2 to free the transition by modifying the phase sequence.

Offsets were chosen as the subject to optimize for both FTC and SAC using the signal timing tool Vistro 2020 [41]. For BMPC and MMPC, the offset was calculated based on a time-space diagram that considers the distance and speed between adjacent intersections, as well as the queue service time of the downstream intersection ($\mathrm{QS}_{2,\mathrm{K2}} = 3$ s and $\mathrm{QS}_{3,\mathrm{K2}} = 5$ s). A gap time of 3 s was utilized for SAC.

8.4. Optimization Problem Solving. The optimal prediction model was solved using Pyomo [42] and IPOPT [43].

(1) BMPC: The objective function was defined as $\sum_{n=n_c}^{n_c+N_\mathrm{p}-1} \sum_{\forall i,\mathrm{K}j} (X_{i,\mathrm{K}j}(n)/\mathrm{SC}_{i,\mathrm{K}j})^2$, and constraints (1)–(13) were applied. Given that the results were real numbers, the final green time was determined by rounding. Furthermore, $r_{i,\mathrm{K}j}$ was calculated as the median value of the sampling ranges of the percentage of turning vehicles.

(2) MMPC: The objective function was defined as $\sum_{n=n_c}^{n_c+N_\mathrm{p}-1} \sum_{\forall i,\mathrm{K}j} X_{i,\mathrm{K}j}(n)$, and constraints (2), (4), (7), and (9)–(23) were applied. The remaining steps were the same as for BMPC, the only difference being the use of $\hat{r}_{i,\mathrm{K}j}$ in the calculation instead of $r_{i,\mathrm{K}j}$.

8.5. Simulation Modeling. The parameters of the Wiedemann 74 model, which allow the HCM2010 method [44] to calculate a base saturated flow rate of 1900 veh/h/lane, were chosen. For every control technique, 50 simulation runs were conducted, each consisting of a 900 s warm-up period followed by a 10800 s data analysis period.

8.6. Simulation Results

8.6.1. Experiment 1. In this experiment, the control objectives of MMPC in Sections 5–7 were verified using the mean absolute error (MAE) of the number of vehicles and the actual offset deviation. These performance measures were calculated based on the actual number of vehicles and offset for every cycle. BMPC-A, which shared the same phase sequence as MMPC, was chosen as the benchmark control technique.

The absolute error in the number of vehicles was calculated by comparing the actual and estimated values. The MAE values were averaged for every cycle in the arterial, as presented in Table 7, which demonstrates the effectiveness of MMPC in reducing the MAE compared with BMPC-A, which can be attributed to the introduction of a real-time vehicle distribution ratio and the percent arrival before the end of green. The accurate vehicle distribution ratio facilitated the precise estimation of the number of vehicles for the current cycle, while the constraint modified by the percent arrival before the end of green enhanced the model's consistency with the realistic traffic environment.

The offset of intersection 1 is set to 0. Figure 5 shows the deviation of the actual offset from the initial offset for intersections 2 and 3. Due to the absence of transition, BMPC-A exhibited varying degrees of early return to the green problem there. The transition-free structure in MMPC played a crucial role in maintaining a constant actual offset throughout the control process.

MMPC demonstrated exceptional capabilities in accurately estimating and predicting the traffic state while effectively maintaining the offset at every intersection. Consequently, it was justifiable to anticipate that these distinct advantages of MMPC would yield significant performance enhancements.

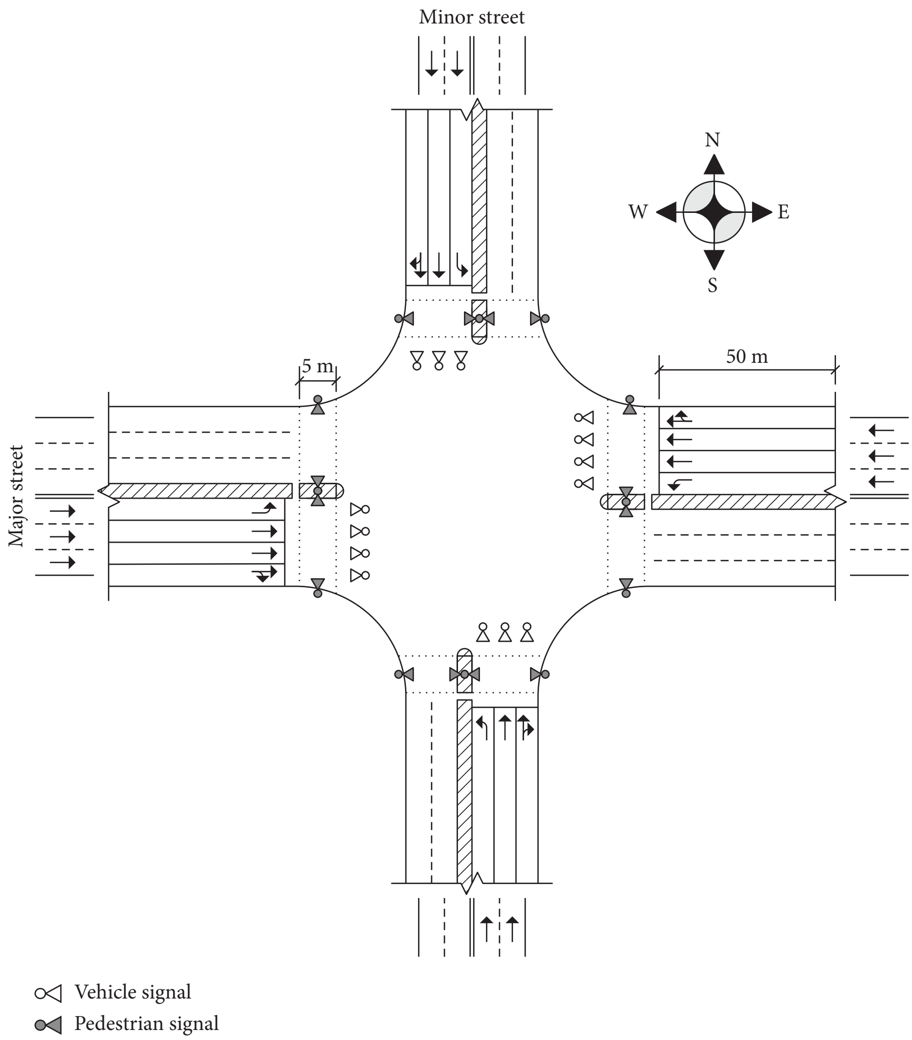

Figure 4: Layout of the test-bed intersection.

Table 4: Sampling ranges of the traffic demand.

Sampling item	Intersections	Approaches	Demand loading period		
			0–2700 s	2700–9900 s	9900–11700 s
Vehicle input (veh/h)	1	West	1100–1300	1700–1900	1100–1300
	3	East	1100–1300	1500–1700	1100–1300
	1, 2, and 3	North and south	400–600	800–1000	400–600
Unidirectional pedestrian input (ped/h)	1, 2, and 3	—	100–200	200–400	100–200

Table 5: Sampling ranges of the percentage of turning vehicles (%).

Movement	Approaches	Sampling points
Left-turn	East and west	10.0, 10.1, . . ., 20.0
	North and south	15.0, 15.1, . . ., 25.0
Right-turn	East and west	5.0, 5.1, . . ., 10.0
	North and south	10.0, 10.1, . . ., 15.0

Table 6: Green time of phases for FTC (s).

Intersection	Phases							
	K1	K2	K3	K4	K5	K6	K7	K8
1	15	33	12	21	19	29	11	22
2	16	31	12	22	17	30	12	22
3	17	30	12	22	16	31	11	23

8.6.2. Experiment 2. The performance measures employed in this experiment comprised: (1) high-priority path travel speed; (2) average vehicle delay; (3) total travel time (TTT); and (4) average number of stops. With the exception of the high-priority path travel speed, all of the performance measures for a given period were averaged across 50 simulation runs.

The travel speed was measured from the stop lines of Phase K2 at intersection 1 to those at intersection 3, following the coordinated direction.

Table 7: Mean absolute error of number of vehicles (veh).

	BMPC-A	MMPC
Current cycle	0.82	0.63 (−22.58%)
Next cycle	4.22	3.29 (−21.88%)

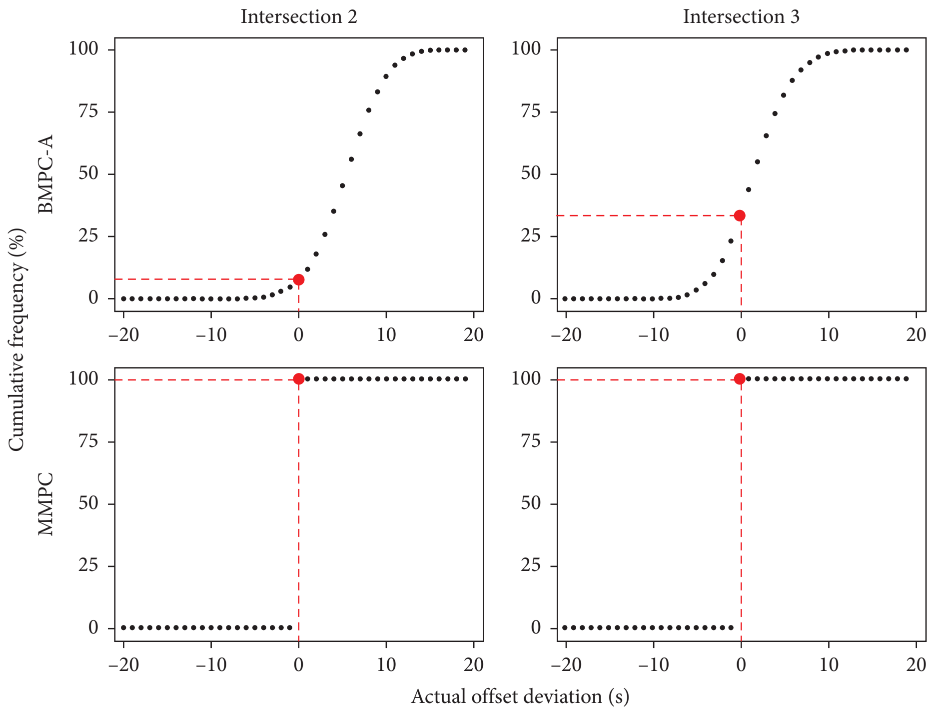

Figure 5: Cumulative frequency distributions of the actual offset deviation.

Figure 6 shows the summary statistics and probability density of the travel speed in a high-priority path. The MPC techniques (BMPC-A, BMPC-B, and MMPC) outperformed the conventional control techniques (FTC and SAC) in terms of the mean travel speed. For the conventional control techniques, the majority of vehicles traveled at speeds less than 30 km/h. MMPC performed better than BMPC-A and BMPC-B in terms of the mean, median, and 15th and 85th percentiles of the travel speeds. Moreover, MMPC had nearly half of the vehicles traveling at speeds greater than 40 km/h.

The measurement zone, which extended from a significant distance away from the stop lines to the beginning of the intersection exit, was used to measure the number of stops and vehicle delay for every vehicle movement. TTT was calculated as the cumulative travel time of all of the vehicles in the arterial.

Tables 8 and 9 demonstrate that the MMPC-enabled arterial outperforms the arterial utilizing other benchmark techniques in terms of system average vehicle delay, TTT, and system average number of stops. This is attributed to MMPC's ability to maintain the performance of major streets at a suboptimal level, while simultaneously optimizing the performance of minor streets to nearly optimal levels.

The computation efficiency of the control techniques was evaluated using the runtime per cycle. In this experiment,

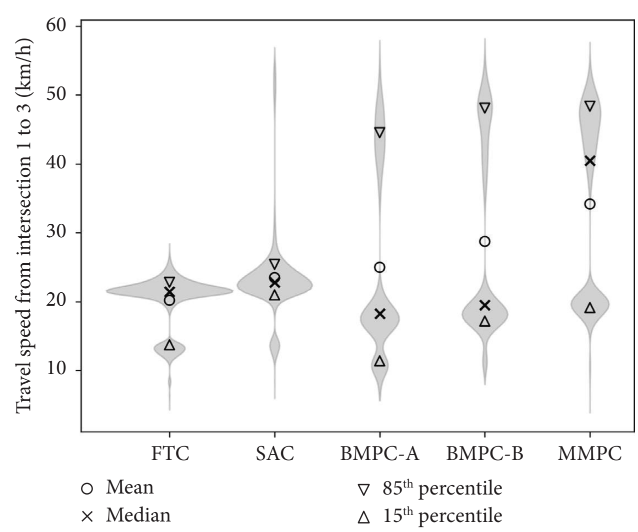

Figure 6: Violin plots of the high-priority path travel speed.

BMPC-A, BMPC-B, and MMPC have average runtimes per cycle of 0.25, 0.25, and 0.35 s, with maximum runtimes per cycle reaching 1.87, 0.91, and 1.22 s, respectively. Compared to BMPC, the average runtime for MMPC increased by 0.1 s. However, it is more important, from the perspective of implementation, whether the maximum runtimes exceed the

Table 8: Average vehicle delay and total travel time.

Control technique	Average vehicle delay (s)			TTT ($\times 10^6$ s)
	System	Major street	Minor street	
FTC	62.73	37.52	109.72	7.24
SAC	56.44	**35.16**	96.11	6.91
BMPC-A	63.61	50.85	87.63	7.18
BMPC-B	67.16	68.69	64.32	7.46
MMPC	**49.19**	42.06	**62.54**	**6.56**

The bold values represent the minimum values for each column, which are also the optimal values.

Table 9: Average number of stops.

Control technique	Average number of stops		
	System	Major street	Minor street
FTC	1.32	0.82	2.26
SAC	1.21	**0.80**	1.97
BMPC-A	1.36	1.12	1.82
BMPC-B	1.38	1.38	**1.39**
MMPC	**1.06**	0.87	1.40

The bold values represent the minimum values for each column, which are also the optimal values.

threshold value. In traffic signal control, the green time of the phase needs to satisfy the minimum green. Therefore, the signal controller does not need to determine the timing plan at the beginning of the cycle; instead, it should be determined at the latest when the minimum green is first satisfied. According to the definition of the minimum green, this threshold is at least 5 s. This ensures that the signal controller employing the mentioned techniques can obtain the timing plan in a timely manner while satisfying all the basic conditions for implementation.

9. Conclusions

This paper proposes modified model predictive control (MMPC) for coordinated signals along an arterial, with the aim of approximating the realistic traffic environment. The modifications proposed in this paper, namely, the transition-free ring-barrier structure, vehicle distribution ratio, and percent arrival before the end of green; collectively contribute to the distinctive characteristics of MMPC. The simulation results demonstrate that MMPC effectively maintains coordination without the need for transition and accurately estimates current and future traffic states by employing modified constraints. These findings highlight MMPC's ability to closely approximate real-world traffic environments. MMPC outperforms the benchmark techniques in terms of vehicle progression for coordinated movement, resulting in significant system-wide improvements in delays, number of stops, and TTT, with only a minor and acceptable increase in runtime.

Certainly, there is still significant potential for improving the performance of MMPC. Future research should focus on integrating real-time percent arrivals before the end of green into the optimization problem. Strictly speaking, MMPC only accomplishes a part of the signal control process, i.e., splits, because the offset and cycle length are still to be determined using other techniques. Hence, future research should also explore the utilization of reinforcement learning to generate signal cycle lengths, where MMPC can contribute as prior knowledge to expedite the training process. Significantly, this research transcends the confines of typical assumptions and large-scale traffic networks, exploring a new avenue to drive the implementation of MPC in signal control.

Data Availability

The traffic demands used to support the findings of this study are included within the article.

Conflicts of Interest

The authors declare that they have no conflicts of interest.

Acknowledgments

The authors would like to thank the National Natural Science Foundation of China under Grant 61374193.

References

[1] M. Abbas, D. Bullock, and L. Head, "Real-time offset transitioning algorithm for coordinating traffic signals," *Transportation Research Record: Journal of the Transportation Research Board*, vol. 1748, no. 1, pp. 26–39, 2001.

[2] H. Hu and H. X. Liu, "Arterial offset optimization using archived high-resolution traffic signal data," *Transportation Research Part C: Emerging Technologies*, vol. 37, pp. 131–144, 2013.

[3] E. F. Camacho and C. Bordons, *Model Predictive Control*, Springer, London, UK, 2nd edition, 2007.

[4] A. Stevanovic, *Adaptive Traffic Control Systems: Domestic and Foreign State of Practice*, Transportation Research Board, Washington, DC, USA, 2010.

[5] Y. Ren, H. Jiang, L. Zhang, R. Liu, and H. Yu, "HD-RMPC: a hierarchical distributed and robust model predictive control framework for urban traffic signal timing," *Journal of Advanced Transportation*, vol. 2022, Article ID 8131897, 14 pages, 2022.

[6] K. Aboudolas, M. Papageorgiou, A. Kouvelas, and E. Kosmatopoulos, "A rolling-horizon quadratic-programming approach to the signal control problem in large-scale congested urban road networks," *Transportation Research Part C: Emerging Technologies*, vol. 18, no. 5, pp. 680–694, 2010.

[7] M. Schwenzer, M. Ay, T. Bergs, and D. Abel, "Review on model predictive control: an engineering perspective," *International Journal of Advanced Manufacturing Technology*, vol. 117, no. 5-6, pp. 1327–1349, 2021.

[8] Z. Zhou, B. De Schutter, S. Lin, and Y. Xi, "Multi-agent model-based predictive control for large-scale urban traffic networks using a serial scheme," *IET Control Theory and Applications*, vol. 9, no. 3, pp. 475–484, 2015.

[9] D. Ma, J. Xiao, and X. Ma, "A decentralized model predictive traffic signal control method with fixed phase sequence for urban networks," *Journal of Intelligent Transportation Systems*, vol. 25, no. 5, pp. 455–468, 2020.

[10] L. Adacher and M. Tiriolo, "Performance analysis of decentralized vs centralized control for the traffic signal synchronization problem," *Journal of Advanced Transportation*, vol. 2020, Article ID e8873962, 19 pages, 2020.

[11] A. H. F. Chow, R. Sha, and S. Li, "Centralised and decentralised signal timing optimisation approaches for network traffic control," *Transportation Research Part C: Emerging Technologies*, vol. 113, pp. 108–123, 2020.

[12] C. Zhang, T. Z. Qiu, and A. Kim, "Centralized and decentralized signal control with short-term origin-destination demand for network traffic," *Journal of Advanced Transportation*, vol. 2022, Article ID 5806160, 23 pages, 2022.

[13] F. Storani, R. Di Pace, and B. De Schutter, "A traffic responsive control framework for signalized junctions based on hybrid traffic flow representation," *Journal of Intelligent Transportation Systems*, vol. 27, no. 5, pp. 606–625, 2023.

[14] B.-L. Ye, W. Wu, K. Ruan et al., "A survey of model predictive control methods for traffic signal control," *IEEE/CAA Journal of Automatica Sinica*, vol. 6, no. 3, pp. 623–640, 2019.

[15] A. Kouvelas, K. Aboudolas, M. Papageorgiou, and E. B. Kosmatopoulos, "A hybrid strategy for real-time traffic signal control of urban road networks," *IEEE Transactions on Intelligent Transportation Systems*, vol. 12, no. 3, pp. 884–894, 2011.

[16] L. Pedroso and P. Batista, "Decentralized store-and-forward based strategies for the signal control problem in large-scale congested urban road networks," *Transportation Research Part C: Emerging Technologies*, vol. 132, Article ID 103412, 2021.

[17] K. Aboudolas, M. Papageorgiou, and E. Kosmatopoulos, "Store-and-forward based methods for the signal control problem in large-scale congested urban road networks," *Transportation Research Part C: Emerging Technologies*, vol. 17, no. 2, pp. 163–174, 2009.

[18] L. B. de Oliveira and E. Camponogara, "Multi-agent model predictive control of signaling split in urban traffic networks," *Transportation Research Part C: Emerging Technologies*, vol. 18, no. 1, pp. 120–139, 2010.

[19] X. Zhou and Y. Lu, "Coordinate model predictive control with neighbourhood optimisation for a signal split in urban traffic networks," *IET Intelligent Transport Systems*, vol. 6, no. 4, pp. 372–379, 2012.

[20] B.-L. Ye, W. Wu, L. Li, and W. Mao, "A hierarchical model predictive control approach for signal splits optimization in large-scale urban road networks," *IEEE Transactions on Intelligent Transportation Systems*, vol. 17, no. 8, pp. 2182–2192, 2016.

[21] B.-L. Ye, W. Wu, H. Gao, Y. Lu, Q. Cao, and L. Zhu, "Stochastic model predictive control for urban traffic networks," *Applied Sciences*, vol. 7, no. 6, p. 588, 2017.

[22] G. S. van de Weg, H. L. Vu, A. Hegyi, and S. P. Hoogendoorn, "A hierarchical control framework for coordination of intersection signal timings in all traffic regimes," *IEEE Transactions on Intelligent Transportation Systems*, vol. 20, no. 5, pp. 1815–1827, 2019.

[23] S. Lin, B. De Schutter, Y. Xi, and H. Hellendoorn, "Fast model predictive control for urban road networks via MILP," *IEEE Transactions on Intelligent Transportation Systems*, vol. 12, no. 3, pp. 846–856, 2011.

[24] T. Tettamanti, T. Luspay, B. Kulcsar, T. Peni, and I. Varga, "Robust control for urban road traffic networks," *IEEE Transactions on Intelligent Transportation Systems*, vol. 15, no. 1, pp. 385–398, 2014.

[25] S. Jin, Z. Hou, R. Chi, and X. Bu, "Model free adaptive predictive control approach for phase splits of urban traffic network," in *Proceedings of the Chinese Control and Decision Conference (CCDC)*, pp. 5750–5754, IEEE, Yinchuan, China, May 2016.

[26] K. Lu, P. Du, J. Cao, Q. Zou, T. He, and W. Huang, "A novel traffic signal split approach based on explicit model predictive control," *Mathematics and Computers in Simulation*, vol. 155, pp. 105–114, 2019.

[27] Q. Wang and M. Abbas, "Optimal urban traffic model predictive control for NEMA standards," *Transportation Research Record: Journal of the Transportation Research Board*, vol. 2673, no. 7, pp. 413–424, 2019.

[28] H. Yu and Z. Hou, "Two-level hierarchical optimal control for urban traffic networks," *Transportmetrica: Transportation Science*, vol. 18, no. 1, pp. 144–165, 2020.

[29] D. Ma, J. Xiao, X. Song, X. Ma, and S. Jin, "A back-pressure-based model with fixed phase sequences for traffic signal optimization under oversaturated networks," *IEEE Transactions on Intelligent Transportation Systems*, vol. 22, no. 9, pp. 5577–5588, 2021.

[30] K. Stoilova and T. Stoilov, "Model predictive traffic control by bi-level optimization," *Applied Sciences*, vol. 12, no. 9, p. 4147, 2022.

[31] S. Lin, B. De Schutter, Y. Xi, and H. Hellendoorn, "Efficient network-wide model-based predictive control for urban traffic networks," *Transportation Research Part C: Emerging Technologies*, vol. 24, pp. 122–140, 2012.

[32] Y. Han, A. Hegyi, Y. Yuan, C. Roncoli, and S. Hoogendoorn, "An extended linear quadratic model predictive control approach for multi-destination urban traffic networks," *IEEE Transactions on Intelligent Transportation Systems*, vol. 20, no. 10, pp. 3647–3660, 2019.

[33] T. Urbanik, A. Tanaka, B. Lozner et al., *Signal Timing Manual*, Transportation Research Board, Washington, DC, USA, 2nd edition, 2015.

[34] R. Peñabaena-Niebles, V. Cantillo, S. Cuentas, and J. L. Moura, "Transition between signal timing plans: a methodological and analytical overview," *Transport Reviews*, vol. 34, no. 3, pp. 356–378, 2014.

[35] M. Zheng, H. Xu, K. Zhang, and R. Yao, "Shortest-way: an improved empirical transition method for signal coordination," *Journal of Advanced Transportation*, vol. 2017, Article ID 7670521, 12 pages, 2017.

[36] H. Xu, K. Zhang, D. Zhang, and Q. Zheng, "Traffic-responsive control technique for fully-actuated coordinated signals," *IEEE Transactions on Intelligent Transportation Systems*, vol. 23, no. 6, pp. 5460–5469, 2022.

[37] L. A. Klein, M. K. Mills, and D. R. Gibson, "Traffic detector handbook: third edition—volume I," federal highway administration," Technical. Report. FHWA-HRT-06-108, 2006.

[38] P. Emami, L. Elefteriadou, and S. Ranka, "Long-range multi-object tracking at traffic intersections on low-power devices," *IEEE Transactions on Intelligent Transportation Systems*, vol. 23, no. 3, pp. 2482–2493, 2022.

[39] B. Yang, H. Zhang, M. Du, A. Wang, and K. Xiong, "Urban traffic congestion alleviation system based on millimeter wave radar and improved probabilistic neural network," *IET Radar, Sonar and Navigation*, 2023.

[40] German Road and Transportation Research Association, *Guidelines for Traffic Signals- English Version of RiLSA*, German Road and Transportation Research Association (FGSV), Germany, 2021.

[41] Ptv Ag, *Vistro 2020 User Manual*, PTV AG, Karlsruhe, Germany, 2020.

[42] M. L. Bynum, G. A. Hackebeil, W. E. Hart et al., *Pyomo–Optimization Modeling in Python*, Vol. 67, Springer, Berlin, Germany, 3rd edition, 2021.

[43] A. Wächter and L. T. Biegler, “On the implementation of an interior-point filter line-search algorithm for large-scale nonlinear programming,” *Mathematical Programming*, vol. 106, no. 1, pp. 25–57, 2006.

[44] Transportation Research Board, *HCM 2010: Highway Capacity Manual*, Transportation Research Board, Washington, DC, USA, 2010.